JTTEE5 12:265-281

On Some Aspects of Gas Dynamics of the Cold Spray Process

V.F. Kosarev, S.V. Klinkov, A.P. Alkhimov, and A.N. Papyrin

(Submitted 21 December 2001; in revised form 2 April 2002)

This paper presents an overview of results of recent studies conducted at the Institute of Theoretical and Applied Mechanics of the Siberian Division of the Russian Academy of Science in the field of gas dynamics and heat transfer of the supersonic air jet under conditions typically used in the cold spray process. These studies are related to various aspects of the problem including a flow in the nozzle and the outflow of the jet, as well as effects of the interaction of the jet with a flat obstacle. They are conducted with a supersonic nozzle with a rectangular section at the exit with a Mach number M_0 between 2 and 3.5. The gas flow in the nozzle is theoretically and experimentally studied. It is shown that the boundary layer on the walls of the nozzle affects significantly the flow parameters (for example, Mach number M, pressure p, temperature T, and density ρ of the gas). A method of calculation of the gas parameters in the flow core of the nozzle is suggested, and it is shown that they depend mainly on the ratio of the nozzle width to its length. The results of the investigation of the supersonic air jets with stagnation temperature ranging from 300-600 K flowing in the atmosphere are presented. The corresponding dimensions of the jets, profiles, and axial distributions of the gas parameters are obtained. The interactions of the supersonic jet with the flat obstacle are studied. Self-similarity of the distribution of the pressure and of the Mach number on the obstacle surface is shown for the jets with various values of the Mach number and the angle of impingement. The oscillation regimen of the jet impingement, as well as a compressed layer structure is observed with the aid of a Schliren visualization technique. Some problems of heat exchange of the jets with the obstacle are considered. Distributions of stagnation temperature and heat exchange coefficient in the near-wall jet are obtained. The temperature of the obstacle for the stationary case is calculated, and it is shown that for heat conductive materials the surface temperature is lower than the stagnation temperature due to the redistribution of heat inside of the substrate.

Keywords boundary layer, cold spray, heat transfer, Mach number, nozzle, supersonic jet

1. Introduction

The cold gas-dynamic spray method (CGSM, or simply cold spray) is based on the selection of a combination of particle temperature, velocity, and size allowing spray coatings at the lowest temperature possible. In the cold spray process, powder particles (1-50 μm) are accelerated to velocities between 300 and 1200 m/s by the supersonic gas jet at a temperature always lower than the melting temperature of the spraying material therefore providing the coating formation from particles in solid state. As a consequence, the deleterious effects of oxidation, evaporation, melting, crystallization, residual stresses, debonding, gas release, and other common problems in traditional thermal spray methods can be avoided.

Originally, the cold spray process was developed in the mid-1980s at the Institute of Theoretical and Applied Mechanics of the Russian Academy of Science in Novosibirsk by A. Papyrin and colleagues.[1-5] They successfully deposited a wide range of pure metals, metal alloys, and composites onto a variety of substrate materials and demonstrated the feasibility of cold spray for various applications. A U.S. patent on the cold spray technology was issued in 1994,[6] and a European one in 1995.[7]

V.F. Kosarev, S.V. Klinkov, and **A.P. Alkhimov,** Institute of Theoretical and Applied Mechanics of Russian Academy of Science, Russia; and **A.N. Papyrin,** Ktech Corporation, 2201 Buena Vista SE, Suite 400, Albuquerque, NM. Contact e-mail: papyrin@ktech.com.

In the USA, the first research in the field of cold spray was conducted in 1994-95[8,9] by a consortium formed under the auspices of the National Center for Manufacturing Sciences (NCMS) of Ann Arbor, MI. Presently, a wide spectrum of research on the cold spray process is being conducted at several research centers including the Institute of Theoretical and Applied Mechanics of the Russian Academy of Science,[10-18] Sandia National Laboratories,[19-25] the Pennsylvania State University,[26-29] ASB Industries, Inc.,[30,31] Ford Motor Company,[32] Thayer School of Engineering, Dartmouth College,[33,37] Rutgers University,[34] University of Bundeswehr, Germany,[35-37] European Aeronautic Defense and Space Company, Germany,[38] Shinshu University, Japan,[39] and others.

The results of these studies related to the jet gas dynamics,[10,14-16,18-20,22-25,33,34,37] and physics of high-speed particle impact,[13,17,21,38] as well as spraying various powder materials and developing specific technologies[12,17,26-32,40,41] are very important for understanding the process and developing commercial applications. At the same time, it should be noted that some questions are not fully answered and among them is a problem of optimization of the jet gas dynamics.

There are several aspects to this problem, and one of the most important tasks of the optimization is to provide a particle velocity as high as possible. Some results of calculation and measurement of particle velocity are presented in Ref. 10, 19, 20, 25, 33, 34, 38, and 39. A detailed analysis of the various factors, which can influence the particle velocity in the cold spray process, is made in Ref. 19. An analytical model using the one-dimensional isentropic flow approximation is used, and results on the nozzle shape optimization are presented.

However, it should be noted that some important factors, which can greatly influence the jet gas dynamics, have not been studied thoroughly at the present time. Among such factors are the boundary layer on the nozzle walls, the high-pressure region in the front of the substrate, the structure and stability of the jet exhausting from the nozzle at different regimes, and the interactions of the supersonic jet with the substrate including heat transfer process between the jet and the substrate. All these questions should be answered to provide the optimum particle velocity and temperature at the moment of the particle impact into the substrate.

The objective of the present investigation is to study some gas dynamics and thermal effects related to the supersonic gas

Nomenclature

a	gas sound speed
a_{cr}	critical sound velocity – sound velocity in point where M = 1
b	size of nozzle critical section which is parallel to H
c	heat capacity
c_f	friction coefficient
F_f	friction force per unit length of the nozzle
H	large transverse dimensions of the jet at the nozzle exit
h	small transverse dimensions of the jet at the nozzle exit
H_1	ratio of the displacement thickness to the momentum thickness
L	supersonic part nozzle length
L_w	obstacle length
M	Mach number
M_*	axial Mach number at the nozzle exit
M_c	calculate axial Mach number of gas flow at the nozzle exit
M_{exp}	experimental measured axial Mach number of gas flow at the nozzle exit
M_0	Mach number of isentropic gas flow at the nozzle exit
M_m	axial Mach number
M_{av}	averaged Mach number over nozzle cross-section
n	jet pressure ratio
P	nozzle exit perimeter
p	static pressure
p_*	static pressure at the nozzle exit
p_a	ambient pressure
p_0	stagnation pressure
p_0'	dynamic pressure
p_s	pressure on the obstacle surface
p_{sm}	pressure on the obstacle surface at $x = 0$
Pr	Prandtle number
Re_T**	Reynolds number constructed by energy loss thickness
S	area of the nozzle cross-section
S_{cr}	geometric area in the nozzle throat
S_{exit}	geometric area in the exit cross-section
S_{eff}	effective area in the exit cross-section
$(S_{exit}/S_{cr})_{eff}$	effective ratio of cross-sections
St	Stanton number
T_0	stagnation temperature
T_{0m}	axial stagnation temperature
T_0^*	axial stagnation temperature at nozzle exit
T_a	ambient temperature
T	obstacle temperature
T_s	surface temperature
u	gas velocity along x-axis
u_e	gas velocity in the near-wall jet
v	gas velocity along z-axis
v_{av}	averaged gas velocity over nozzle cross-section
v_m	axial velocity
v^*	velocity at the edge of the laminar sublayer
v_{id}	ideal gas velocity
x	coordinate counted off from the wall to the nozzle axis parallel to h
$x_{0.5}$	half-width of the pressure profile
x_{cr}	coordinate of the sound speed transition
y	coordinate counted off from the wall to the nozzle axis parallel to H
z	coordinate along the nozzle axis
z_0	standoff distance
$z_{0.5}$	M^2 profile thickness, defined by $M^2(z_{0.5}) = 0.5M_m^2$
$z_{0.5}^M$	length of longitudinal Mach distribution, defined by $M_m^2(z_{0.5}^M) = 0.5M_*^2$
$z_{0.5}^T$	length of longitudinal temperature distribution, defined by $\Delta T_{0m}^2(z_{0.5}^T) = 0.5\Delta T_{0*}^2$
$z_{0.5}^w$	M^2 profile thickness in near-wall jet, defined by $M^2(z_{0.5}^w) = 0.5M_m^2$
z_w	compressed layer thickness

Greek symbols

α	heat exchange coefficient
β	velocity gradient near the stagnation point
χ	temperature conductivity coefficient
δ	boundary layer thickness
δ^*	displacement thickness
δ^{**}	momentum thickness
δ_M	jet thickness along x-axis, defined by $M^2(\delta_M) = 0.5M_m^2$
δ_v	velocity profile thickness along x-axis, defined by $v(\delta_v) = 0.5v_m$
τ	non-dimensional time
ξ	non-dimensional coordinate
δ_T	temperature profile thickness along x-axis, defined by $\Delta T_0(\delta_T) = 0.5\Delta T_{0m}$
δ_s	obstacle thickness
γ	specific heat ratio
λ	heat conduction coefficient
μ	viscosity
ρ	gas density
ρ_m	axial gas density
τ_w	shear stress
θ	non-dimensional temperature
φ	bulk concentration of the particles

jet coming from a nozzle with a rectangular cross section and its interaction with the substrate in the cold spray process. It should be noted that nozzles of two types are used under the cold spray process: nozzles with round and rectangular cross section. At the same ratio of the exit and critical cross sections, nozzles with a rectangular section can provide, on one hand, a wider spray beam in the direction of smaller size of the section and, on the other hand, a more narrow beam (to 1-2 mm) in the direction of larger size of the section. Such nozzles can also decrease the effect of the particle deceleration in the compressed layer in front of the substrate due to decreasing thickness of the layer.[10]

Unusual nozzle shape (the great value of the ratio between the length of the supersonic part of the nozzle and the minimum exit dimension) leads to the formation of jets that differ considerably from well-known axisymmetric jets with a uniform distribution of gas parameters at the nozzle exit. Since the axial velocity of the gas rapidly decreases behind the potential core, the initial supersonic region of the jet is of major interest for the spraying practice. In a number of practical applications it is necessary to vary the spraying distance. A question then arises: at what limits are can spray without substantial distortion of the spraying process and changes in coating properties?

This paper presents an overview of results of recent studies conducted at the Institute of Theoretical and Applied Mechanics of the Siberian Division of the Russian Academy of Science in the field of gas dynamics and heat transfer of the supersonic air jet under conditions of the cold spray process.[5,10,11,14-18]

2. Internal Flow

2.1 Experimental Determination of the Gas Flow Parameters at the Nozzle Exit

Nozzles with a conical subsonic part and a plane supersonic part of length L = 50-200 mm, throat size $b \times h$, and exit size $H \times h$ (h = 1-5 mm) are used. The experimental parameters controlled directly by the operator of the system are the stagnation temperature T_0, the pressure in the plenum chamber (stagnation pressure) p_0, the static pressure p at the nozzle exit, and the dynamic pressure p_0' measured by the Pitot tube. The experiments have shown that the stagnation pressure at the axis of the examined nozzles decreases in range about 5%, and the Mach number M_{exp} at the nozzle exit is significantly lower than M_0 (Mach number corresponding to the ideal gas flow) by 10-20%. This difference can be explained by the boundary layer effect on the flow core. From the obtained values of M_{exp}, we evaluated the effective ratio of cross-sections $(S_{exit}/S_{cr})_{eff}$. Assuming the effective throat area to be equal to the geometric area because the boundary layer thickness is extremely small here,[42] the effective area in the exit cross-section S_{eff}, and the boundary layer thickness at the nozzle exit was calculated. We calculated the boundary layer displacement thickness at the nozzle exit assuming that it is the same over the entire perimeter:

$$\delta^* = \frac{H + h - \sqrt{(H+h)^2 - 4\Delta S}}{4} \qquad \text{(Eq 1)}$$

where $\Delta S = S_{exit} - S_{eff}$

For $\delta^* << h$ we have

$$\delta^* \approx \frac{\Delta S}{P} = \frac{S_0 - S_{eff}}{2(H+h)}$$

where $p = 2(H + h)$ is the nozzle exit perimeter. For known δ^* and M_{exp}, the boundary layer thickness was estimated from the formula[46]:

$$\frac{\delta^*}{\delta} = 1 - 7\int_0^1 \frac{z^7 dz}{1 + 0.2M_{exp}^2(1 - z^2)} \qquad \text{(Eq 2)}$$

Based on the resultant boundary layer thickness, it was established that either the boundary layers merged or the situation is close to that for the given nozzle dimensions.

2.2 Calculation of the Gas Flow Parameters at the Nozzle Exit

If the boundary layer thickness is not too large, we can assume that the stagnation pressure in the flow core remains the same, and the gas parameters vary in accordance with the isentropic law. The boundary layer effect is equal to the decrease of the nozzle cross-section. Thus, instead of geometric area ratio in the calculated reconstruction of the gas flow parameters in the flow core, we should use the effective ratio. The boundary layer displacement thickness should be calculated by the Karman equation, Eq 3, assuming that it develops on a flat plate located in the flow without heat transfer and with known pressure or velocity gradient along the axis[43]:

$$\frac{d\delta^{**}}{dx} = \frac{c_f}{2} - \frac{\delta^{**}}{v}\frac{dv}{dx}(2 + H_1 - M_o^2) \qquad \text{(Eq 3)}$$

$$\delta^* = \delta^{**}H_1 \qquad \text{(Eq 4)}$$

where δ^{**} is the momentum thickness, and c_f is the friction coefficient defined in Ref. 44. The dependence of the ratio of the displacement thickness to the momentum thickness H_1 on the Mach number was determined by empirical formula[45]:

$$H_1 = 1.4(1 + 0.3M_o^2) \qquad \text{(Eq 5)}$$

Based on the calculation and experimental results, we plotted the dependence M_c/M_0 and M_{exp}/M_0 on the aspect ratio of the nozzle h/L (Fig. 1).

It is seen in Fig. 1 that the relative Mach number in the examined range of M_0 = 2.18-3.45 depends mainly on h/L and dramatically decreases for $h/L \leq 0.025$. The experimental points are in good agreement with the calculation results. The dashed curve refers to $h/L \approx 0.025$ for which, according to estimates, the boundary layers from the opposite walls of the nozzle merge, i.e., $2\delta/h = 1$ (the same in Fig. 3). Thus, the decrease at $h/L \approx 0.025$ can be explained by the merging of the boundary layers, which start to intensively affect the flow parameters inside the core, and the calculation using the above technique becomes incorrect.

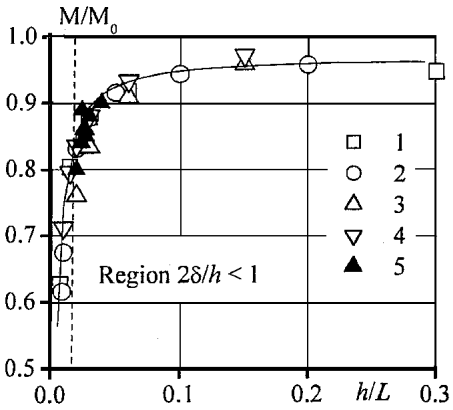

1 – M_0 = 2.72, p_0 = 1.5 MPa, h = 3 mm, b/H = 0.3, b/L = 0.03; L = 10 – 300 mm
2 - M_0 = 2.72, p_0 = 1.5 MPa, L = 0.1 m, b = 3 mm, H = 10 mm; h = 1 – 20 mm
3 - M_0 = 2.18, p_0 = 0.6 MPa, h = 3 mm, b = 3 mm, H = 6 mm; L = 20 – 120 mm
4 - M_0 = 3.45, p_0 = 1.5 MPa, h = 3 mm, b = 3 mm, H = 20 mm; L = 20 – 300 mm
5 - M_0 = 2.0 – 3.35, experimental results.
1 – 4 – M_c/M_0, 5 – M_{exp}/M_0

Fig. 1 Dependency of the relative Mach number at the nozzle exit on relative extension of the nozzle

2.3 Calculation of the Mean Flow Parameters Over the Cross Section and Comparison With the Parameters in the Flow Core

To make the calculation correct, the average gas parameters over the nozzle cross section should be used. The corresponding equation is

$$\frac{dM}{M} = \frac{\left(1 + \frac{\gamma - 1}{2} M^2\right)}{M^2 - 1} \left(\frac{dS}{S} - \frac{\gamma F_f \, dx}{\rho a^2 S}\right) \quad \text{(Eq 6)}$$

$$F_f = c_f \rho v^2 [h + b(x)] \quad \text{(Eq 7)}$$

where all parameters are averaged over the nozzle cross section; c_f is defined in Ref. 44.

The relationship between the mean flow parameters and axial parameters can be obtained assuming the classic law of velocity distribution for the boundary layer[46]:

$$\frac{v}{v^*} = \frac{1}{\kappa} \ln \frac{v^* y}{v} + 5.5 \quad \text{(Eq 8)}$$

where y is the coordinate in the direction perpendicular to the nozzle wall, $v^* = \sqrt{\tau_w/\rho}$ is the velocity at the edge of the laminar sublayer, $\tau_w = c_f \rho v^2/2$ is the shear stress, and k = 0.4 is the universal constant of turbulent flow. This law gives a good description of the gas velocity distribution in cold spray nozzles. This is clearly seen from Fig. 2, which shows a comparison of the distribution obtained experimentally at the nozzle exit and the distribution calculated by (6) for δ/h = 0.4.

2.4 Comparison With the Experiment

Figure 3 shows a comparison of the axial velocity normalized to the ideal gas velocity, which was obtained by Eq 3-5 and 6-8 calculation models. A significant difference between calculation results for the axial velocity in the region $2\delta/h > 1$ shows that the model of Eq 3-5, assuming a constant stagnation pressure at the axis, cannot be used here. In this case, after the boundary layer junction, the axial velocity should be reconstructed by the Eq 6-8 calculation model, taking into account the decrease in stagnation pressure.

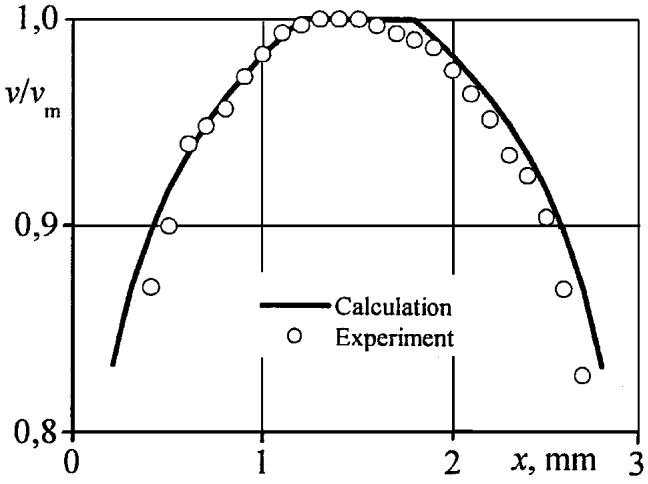

Fig. 2 Velocity distribution at the exit of a supersonic nozzle

In conclusion, we should note that a good agreement of the calculated results for the gas parameters in the flow core in a rectangular supersonic nozzle and the experimental data allows us to calculate the particle acceleration in these nozzles and to design the most optimal nozzles for cold spray.

3. Jet

3.1 Profiles of the Jet Parameters

It is known from Ref. 47-49 that the profiles of velocity (v) and dynamic pressure (ρv^2) are self-similar at the initial and basic regions of the jet. It is convenient to represent the dynamic pressure in the form $\gamma p M^2$, which leads to self-similarity of M^2 profiles in isobaric jet. The M^2 profiles were reconstructed from experimentally obtained profiles of static (p) and dynamic (p_0') pressures. The data obtained when studying the jets with different initial (denoted by *) parameters (h = 1-4.5 mm; H/h = 2.7-8; $M_* = 1.85$-3.1; T_0^* = 300-600 K, where h and H are the small and large transverse dimensions of the jet at the nozzle exit) and

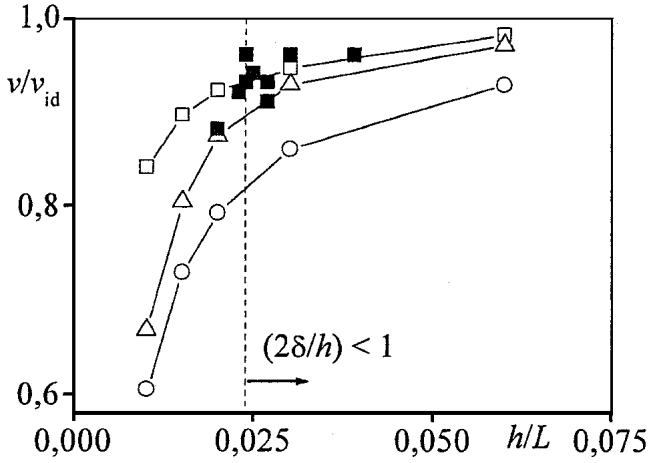

Fig. 3 Gas velocity at the nozzle axis: □, at the axis (without regard for variation of p_0); ○, mean value over the nozzle cross-section; Δ, at the axis (reconstructed from the mean value); ■, experiment

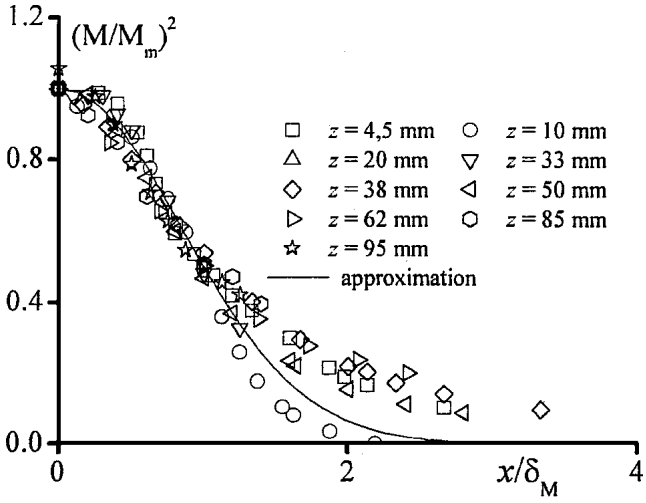

Fig. 4 Normalized M^2 profiles for an overexpanded jet exhausted from the nozzle with h = 4.5, H/h = 2.7, M_* = 3.1

plotted in coordinates $(M/M_m)^2$, x/δ_M fit a single curve (Fig. 4). With an insignificant scatter, this curve can be represented by the function:

$$\varphi_M = \exp[-(0.83x/\delta_M)^2] \quad \text{(Eq 9)}$$

where δ_M is the jet thickness along its smaller size (in the x direction) defined as the distance from the jet axis to the point where $M^2(\delta_M) = 0.5M_m^2$.

The stagnation temperature (T_0) and the jet pressure ratio ($n = p_*/p_a$) in the examined ranges (T_0 = 300-600 K, n = 0.5-1) do not essentially effect the M^2 profile. It is known from the jet theory that the profiles of the stagnation temperature difference ($\Delta T_0 = T_0 - T_a$) are also self-similar allowing for the relationship:

$$(T_0 - T_a)/(T_{0m} - T_a) = \Delta T_0/\Delta T_{0m} = (v/v_m)^\sigma \quad \text{(Eq 10)}$$

where s = 0.5 for plane jets, s = 0.75 for axisymmetric jets, v is the gas velocity, T_a is the ambient temperature. Assuming the profiles to be described by functions of the same form, we can obtain the relation between the velocity profile thickness (δ_v) and the temperature profile thickness (δ_T):

$$\delta_v = \delta_T \sqrt{\sigma} \quad \text{(Eq 11)}$$

We performed a series of experiments to verify self-similarity, to obtain an approximating function of stagnation temperature profiles, and to find the relation between the thicknesses of M^2 and ΔT_0 profiles. Stagnation temperature was measured by a hot-wire probe. The profiles constructed in coordinates $\Delta T_0/\Delta T_{0m}$, x/δ_T fit the curve:

$$\varphi_T = \exp[-(0.83x/\delta_T)^2] \quad \text{(Eq 12)}$$

with a small scatter (Fig. 5). The experimentally found ratio δ_T/δ_M for the examined range of parameters is 2.

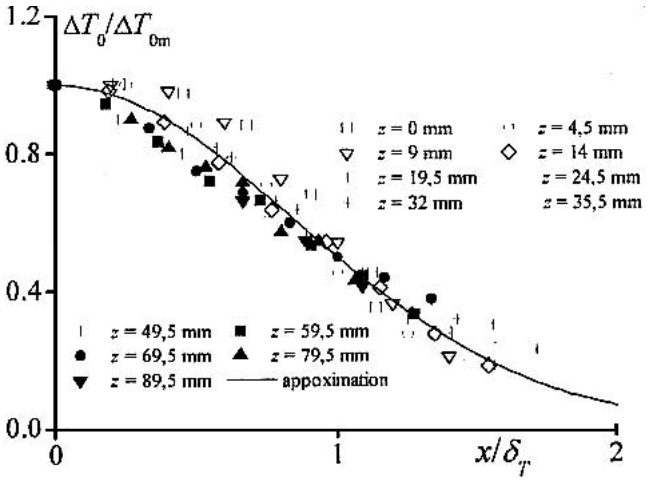

Fig. 5 Normalized profiles of stagnation temperature difference in an overexpanded jet exhausted from the nozzle with h = 4.5, H/h = 2.7, M = 3.1

3.2 The Largest Deviation of the Jet Parameters

We made an attempt to find a smooth approximating function of axial jet parameters denoted here by the subscript m. Figure 6 shows the data from Ref. 46. Similar data obtained in our experiments are presented in Fig. 7. It is seen that all data lie on a single curve of the form:

$$\left(\frac{M_m}{M_*}\right)^2 = \left[1 + 3\left(z/z_{0.5}^M\right)^4\right]^{-0.5} \quad \text{(Eq 13)}$$

where z is the longitudinal coordinate in the jet, $z_{0.5}^M$ is the coordinate where $M_m^2(z_{0.5}^M) = 0.5M_*^2$.

The largest deviation from the above curve is observed for data obtained for an overexpanded jet, though even in this case the upper peaks lie on this curve. It should be noted that approxi-

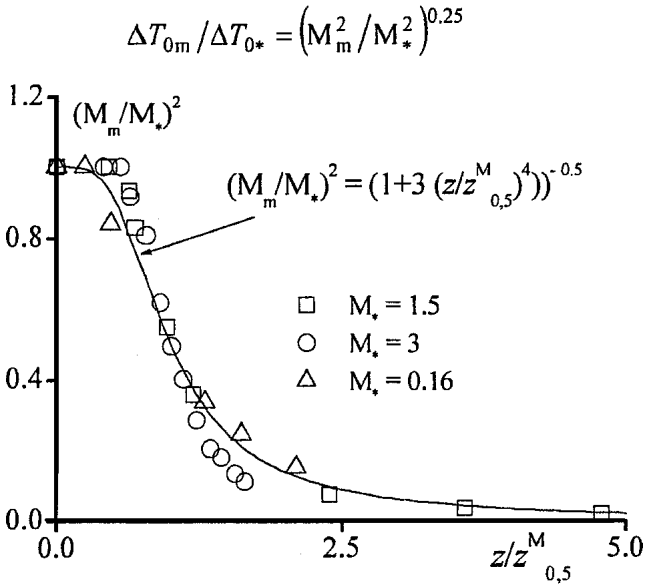

Fig. 6 Generalized dependence for distribution of axial values of M^2 versus the longitudinal coordinate from Ref. 48

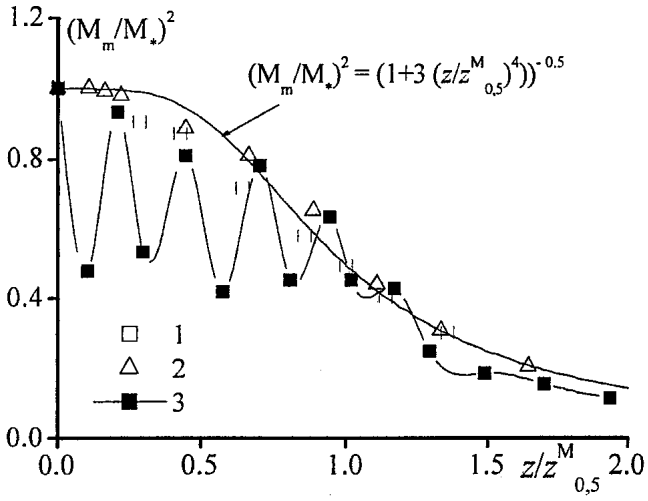

Fig. 7 Generalized dependence for distribution of axial values of M^2 versus the longitudinal coordinate: 1 corresponds to $h = 1$ mm, $M = 1.85$; 2 corresponds to $h = 3$ mm, $M = 2.75$; 3 corresponds to $h = 4.5$ mm, $M = 3.1$, $n = 0.5$

mating function is also asymptotically valid, since according to the momentum conservation equation for axisymmetric jets (as at large distances all jets can be treated as axisymmetric) $M_m^2 \sim 1/z^2$.

It can be shown that for moderate heated jets the relation between the axial stagnation temperature difference and the axial value of M^2 should be close to the form

$$\Delta T_{0m}/\Delta T_{0*} = (M_m^2/M_*^2)^{0.25} \quad \text{(Eq 14)}$$

It is used to find the distribution function of the axial values of the stagnation temperature difference. A comparison with experimental data allows us to write it in the form (Fig. 8):

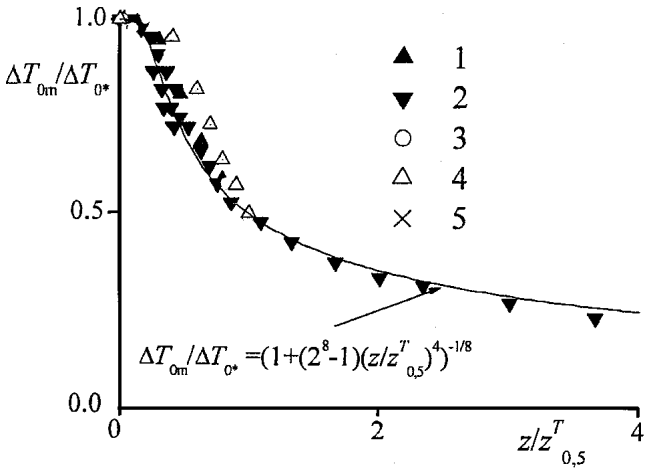

Fig. 8 Generalized dependence of normalized stagnation temperature difference versus the longitudinal coordinate. 1,2 correspond to $h = 1$ m, $M_* = 1.8$, $z^T_{0.5} = 30$ mm; 3 corresponds to $h = 3$ mm, $M_* = 2.6$, $z^T_{0.5} = 90$ mm; 4,5 corresponds to $h = 4.5$ mm, $M_* = 3.1$, $z^T_{0.5} = 100$ mm

$$\Delta T_{0m} = \Delta T_{0*}/[1 + (2^8 - 1)\bar{z}^4]^{1/8}$$

$$\bar{z} = z/z^T_{0.5},\ z^T_{0.5} \approx 2\,z^M_{0.5} \quad (15)$$

The relation $z^T_{0.5}/z^M_{0.5}$ obtained experimentally is equal to 2.

3.3 Jet Thickness

One important problem of the jet theory is the determination of the jet thickness as a function of the longitudinal coordinate. It is known that a linear increase in thickness is observed both in the initial and basic regions of the jet, though with different proportionality coefficients.[48] Thus, there is a transitional region in which the thickness growth is represented by a nonlinear function. Since the jets of nonuniform initial profile are studied due to thick boundary layer on the nozzle walls, it should be expected that the potential core region is weakly expressed. Thus, the jet thickness should be approximated by a nonlinear function. Assuming the jet to be plane, i.e., ignoring its expansion in the larger size direction, we can find the relationship between the jet thickness and the axial value of M^2 from the momentum conservation equation and obtain the formula:

$$\delta_x = h[1 + 3(z/z^M_{0.5})^4]^{0.5} \quad \text{(Eq 16)}$$

If we assume that the jet expansion along the larger size is exactly the same as along the smaller size (symmetric case), i.e., $\delta_y/\delta_x = H/h$ (δ_y is the jet thickness along the larger size), we obtain:

$$\delta_x = h[1 + 3(z/z^M_{0.5})^4]^{0.25} \quad \text{(Eq 17)}$$

Experimental data permit obtaining a more accurate function (Fig. 9):

$$\delta_x = 0.75h[1 + 3(z/z^M_{0.5})^4]^{0.4} \quad \text{(Eq 18)}$$

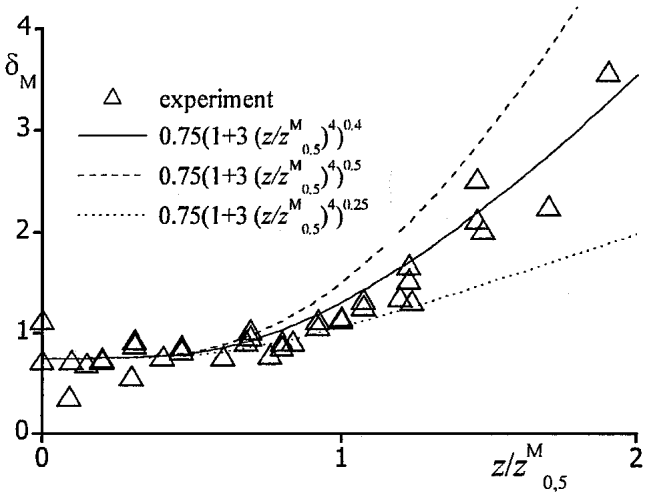

Fig. 9 Generalized dependence of jet thickness versus the longitudinal coordinate

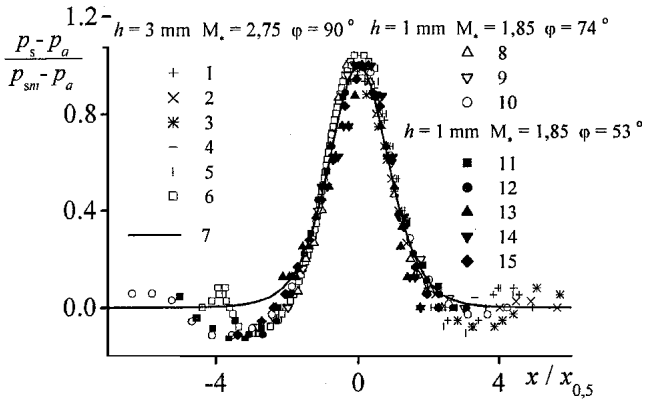

Fig. 10 Pressure profiles on the obstacle surface at the isobaric jet impingement: 1 corresponds to a distance of 6 mm; 2, 9 mm; 3, 12 mm; 4, 15 mm; 5, 1.5 mm; 6, 3 mm; 8, 6 mm; 9, 4 mm; 10, 2 mm; 11, 1 mm; 12, 2 mm; 13, 4 mm; 14, 6 mm; 15, 3 mm; 7, approximation line. Points 1-6 correspond to $h = 3$ mm, $M = 2.75$, $\varphi = 90°$; points 8-15 correspond to $h = 1$ mm, $M = 1.85$, $\varphi = 74°$ (points 8-10) and 53° (points 11-15).

Thus, as should be expected, the examined jets cannot be classified as either plane or symmetric.

The performed study verified the self-similarity of M^2, ΔT_0, and v profiles. The region of self-similarity begins at a certain distance from the nozzle exit and extends downstream without any limitations. The transition through the sonic lines does not have any effect on the profiles of parameters. Due to a considerable thickness of the boundary layer formed at the nozzle walls, the initial profiles can hardly be distinguished from self-similar ones. On these grounds, the region of self-similarity can be extended to the entire jet beginning from the nozzle exit.

It was found that the initial nonuniformity of gas parameters at the nozzle exit leads to a more smooth transition from the initial to the basic region of the jet in the longitudinal distribution of M^2. The measurements of the jet thickness growth have shown that the growth observed in the experiments is smaller than the growth predicted for a plane jet, which is apparently explained by tip effects arising in the jets with a finite ratio of dimensions.

4. Impingement

The experiments are conducted using a set-up including a steel plate as the obstacle with holes 0.2 mm in diameter used to measure the pressure on the obstacle surface. Pressure profiles on the obstacle surface are measured by two inter-normal axis x, y. The beginning of the coordinates is in the center of projection of the rectangular outlet nozzle section to the obstacle surface. The axes of the coordinates x, y are set parallel to the sides of the outlet nozzle section, x is parallel to the smaller side, y is to the greater one, and the z-axis is normal to the surface of the obstacle. A Pitot tube with an inner diameter of 0.2 mm is used to determine the Mach numbers M in the near-wall jet.

4.1 Distribution of Pressure on the Obstacle Surface

One of the problems of the experimental study of the interaction of the jets with the obstacle was to determine the distribution of pressure on the obstacle surface. These data are necessary to restore the properties of the flow inside the compressed layer (presence or absence of the peripheral maxima) and find the distribution of velocity on the outer boundary of the near-wall boundary layer using Bernoulli integral. The normalized profiles of the pressure distribution on the substrate at the impingement at various angles φ and various distances from the nozzle exit to the obstacle are shown in Fig. 10. Here h is the smaller size of the outlet section of the nozzle, z_0 is the distance from the nozzle exit to the obstacle, p_s is the pressure on the obstacle surface, p_{sm} is the pressure on the obstacle surface at $x = 0$, p_a is ambient pressure, $x_{0.5}$ is half-width of the pressure profile $p_s(x_{0.5}) - p_a = 0.5(p_{sm} - p_a)$. The origin of the x, y system is set at the cross point of the jet center and the obstacle surface.

It is seen, that the experimental results are well approximated by the function

$$\frac{p_s - p_a}{p_{sm} - p_a} = \left[1 + b\left(\frac{x}{x_{0.5}}\right)^2\right]^{-4} \qquad \text{(Eq 19)}$$

where $b = 2^{1/4} - 1 \approx 0.19$ which is taken from Ref. 50, where the self-similarity of pressure distribution on the obstacle surface is affirmed. Value $x_{0.5}$ for $z_0 \leq 4h$ is approximately half of h. Data in the figure show that in this case the self-similarity is observed along the jet of smaller size for the angles $\varphi = 50$-$90°$.

The pressure profiles along the greater axis of the outlet section of the nozzle H are given in Fig. 11. It shows that there is a zone of constant pressure values (at small z_0) and it falls to zero at the edges. Thus, one can say that the distribution of pressure along the y axis is not self-similar, on the one hand, and it can be considered constant at high H/h, on the other hand.

The velocity gradient in the stagnation point along the x-axis can be found with the aid of the surface pressure profiles, Eq 19, using also isentropic formulas for velocity and pressure. As a result we obtain the expression for the velocity gradient near the stagnation point

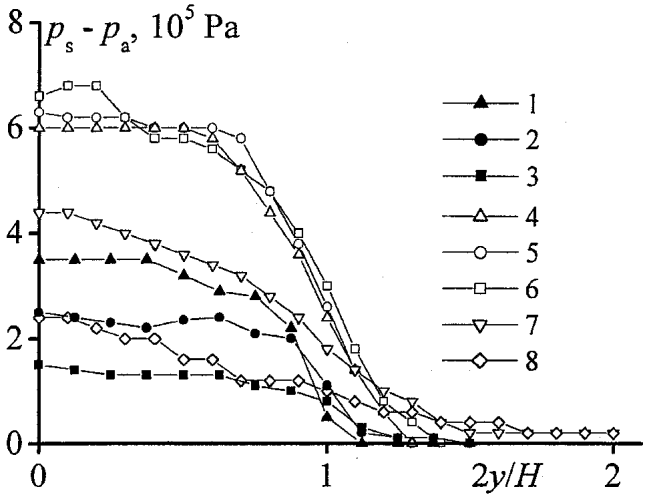

Fig. 11 Pressure profile on the obstacle surface along the greater size of the jet section at the impingement of isobaric jet exhausting from the rectangular nozzle; 1, distance is 2 mm; 2, 4 mm; 3, 6 mm; 4, 2 mm; 5, 5 mm; 6, 9 mm; 7, 15 mm; 8, 30 mm. Points 1-3 correspond to $M = 1.85$, $h = 1$ mm, $H = 8$ mm; points 4-8 correspond to $M = 2.5$, $h = 3$ mm, $H = 10$ mm.

$$\frac{du}{dx} = 2\frac{a_{cr}}{x_{0.5}}\sqrt{\frac{\gamma+1}{\gamma}b\left(1-\frac{p_a}{p_0'}\right)} \qquad \text{(Eq 20)}$$

where a_{cr} is critical velocity of the sound, p_0' is dynamic pressure in the jet (equal stagnation pressure after the bow shock). The value of the root in the right part of the equation for the typical Mach number $M = 1.8$-3.3 is 0.5 with the accuracy 5%. Hence, the velocity gradient can be evaluated with the accuracy sufficient for the practice by the expression

$$\beta = \frac{du}{dx} = \frac{a_{cr}}{x_{0.5}} \approx 2\frac{a_{cr}}{h} \qquad \text{(Eq 21)}$$

From Eq 19 we find the connection between the x_{cr} coordinate of the sound speed transition and the $x_{0.5}$ coordinate. The expression is dependent on the Mach number and nozzle pressure ratio but for the noted range $M = 1.8$-3.3 in case of the impingement of the isobaric jet with the accuracy of not more than 5% it can be evaluated as $x_{0.5}/x_{cr} = 0.87$. Thus, the critical parameters of the gas, when it accelerates along the surface, are reached near the boundary of the falling jet.

4.2 Comparing the Dynamic Pressure Distribution in the Free Jet and the Pressure Distribution on the Obstacle Surface

From Fig. 12 one can see that they are close (z_0 is a distance from the nozzle exit to the obstacle and the inlet hole of the Pitot tube). Thus, to find the pressure distribution along the obstacle surface it is necessary to know the pressure in the center and the thickness $x_{0.5}$ depending on z_0 only. It follows from the data mentioned above that $x_{0.5}$ can be assumed equal to the same size of the free jet. The pressure in the center of the obstacle can be

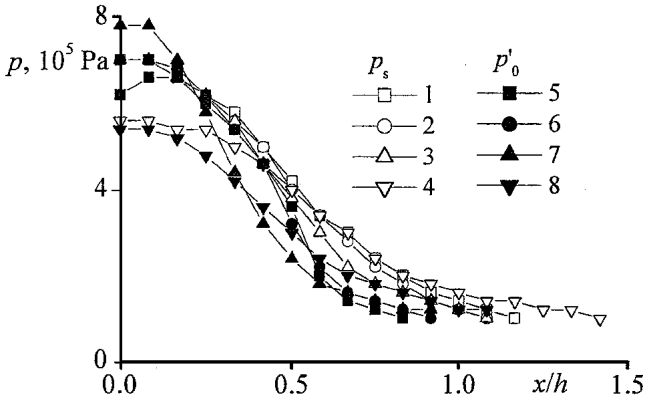

Fig. 12 Pressure profile on the obstacle surface p_s and behind the bow shock wave p_0' along the smaller size of the jet cross section at the impingement of the air isobaric jet exhausting from the rectangular nozzle; $h = 3$ mm, $H/h = 3.3$, M* = 2.5, j = 90°; for 1 and 5, distance is 2 mm; 2 and 6, 9 mm; 3 and 7, 15 mm; 4 and 8, 30 mm

evaluated by the axial pressure in the free jet behind the bow shock.

The distributions of maximum pressure behind the shock wave in the free jet and on the surface mounted at the angle 90° to the jet axis are presented in Fig. 13. If the flow of the ideal gas is considered then the pressure p_s must be equal exactly to the pressure p_0'.

It is shown that at the initial region mean values p_0' and p_s coincide. However, at distance $z_0 \approx 7h$ in the free jet the pressure does not decrease considerably and in the average is equal to the pressure near the nozzle exit. At the same time, under the condition of impingement on the substrate the pressure is approximately two times lower than at the nozzle exit. Thus, the introduction of the substrate makes some changes in the flow structure, though at the region $z_0 \leq 4h$ and $z_0 \geq 15h$ p_0' and p_s coincide.

4.3 Oscillations of the Jet

Probably, this decrease of the surface pressure p_s is connected with the appearance of oscillations of the jet flowing onto the obstacle. Due to these oscillations the amount of air mixed with the jet is increased. This leads to the sharp decrease of the surface pressure p_s. The pictures made with the help of the Schliren visualization system (Fig. 14) show that at some distance from the nozzle exit the instability of the jet is observed. The average length of undisturbed region is about 2-6 times the jet thickness. It should be noted that the amplitude of oscillations increases downstream and reaches 2-3 times the jet thickness. The improvement of the stability is observed when the pressure is increased in the plenum chamber and the regimen of exhaustion is transferred into the non-isobaric one at $n > 1$ (see, for example, Fig. 20).

The problem whether it is possible to avoid oscillations is not clear. This effect is not studied in detail in this paper. It is not clear what is the influence of this phenomenon on the spraying process, namely: if the loading of the powder can change the form of the jet and if not, what is the efficiency of the acceleration of the particles in this jet, how the coefficient of deposition

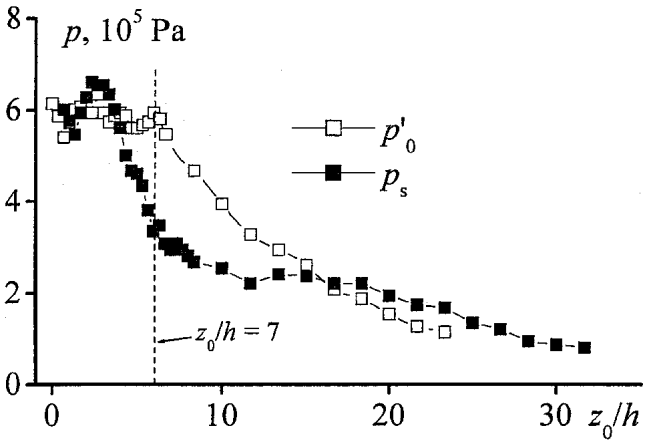

Fig. 13 Dependence of the maximum pressure on the obstacle surface mounted at 90° to the jet axis and behind the bow shock on the standoff distance at the impingement of the air isobaric jet (T_0 = 300 K, p_0^* = 1.4 MPa), exhausting from the rectangular nozzle (h = 3 mm)

varies, how the conditions of deceleration of particles in the constantly deformed shock (impact) layer vary. All these problems should be considered in the future. However, it should be taken into account that in practice the distances for spraying are chosen such that jet instability does not have time to develop.

4.4 Near-Wall Jet

One of the main problems of the research conducted was to obtain the profiles M^2 in the near-wall jet. In the near-wall jet where the static pressure was close to ambient pressure value M^2 was determined by the Rayleigh formula:

$$\frac{p_0'}{p_a} = \left(\frac{k+1}{2}\right)^{(k+1)/(k-1)} M^2 \left(\frac{M^2}{kM^2 - \frac{k-1}{2}}\right)^{1/(k-1)} \quad \text{(Eq 22)}$$

The results of these measurements are presented in Fig. 15.

The analysis of Fig. 15 shows that the near-wall boundary layer on the obstacle surface does not have time to develop considerably (at least it appears to be thinner than the size of the Pitot tube) and the jet boundary layer occupies the main part of it.

To check the self-similarity, the normalized profiles M^2 are shown in Fig. 16. Some difference of these profiles is observed, at the same time they are approximated by the function:

$$M^2/M_m^2 = \exp\left[-\left(0.83\,\frac{z}{z_{0.5}}\right)^2\right] \quad \text{(Eq 23)}$$

To find the values of the Mach numbers in the region of the compressed layer (near the critical point) the results of the surface pressure measurement p_s were used. The M_m^2 distributions along the x-axis of the obstacle surface corresponding to the maximum velocity in the near-wall jet are presented in Fig. 17. It is seen that gas is accelerated till supersonic velocities up to the distance x^* = (2-3)h and then it decelerates.

Thus, it is shown that the distribution of pressure along the surface of the obstacle along the smaller size of nozzle is self-similar in the classic regimen of the impingement and does not depend on the angle of encounting at φ = 50-90°. The critical parameters of the gas, when it accelerates along the surface, are reached near the boundary of the falling jet. The velocity gradient in the critical point can be determined by the formula $\beta = 2a_{cr}/h$. Within a small distance of the obstacle from the nozzle exit ($z_0/h \le 5$) the gas parameters can be considered constant and equal to the parameters at the exit. The study of the near-wall jet have shown that the profiles of velocity and the Mach number are self-similar and maximum gas velocity achieves at x^* = (2-3)h.

4.5 Compressed Layer Thickness

The compressed layer was studied with the aid of the Schlieren visualization. The results of measurement of the layer thickness are presented in Fig. 18 and 19. The layer thickness and stand off distance are normalized by nozzle thickness.

It is seen that at isobaric exhaustion as the first approximation it is possible to assume hat the compressed layer thickness is a constant value equal to half of the jet size. Under a non-isobaric exhaustion, the situation is changed. It allows explanation the interference of the jet wave structure with the bow shock wave. It is exhibited especially at the great jet pressure ratio. The compressed layer structure can be seen in the photos shown in Fig. 20.

A rough estimate of the compressed layer thickness will be made. Jet momentum conservation equation with the account for self-similarity of M^2 profile is

$$\frac{hH}{4}\rho_m v_m \int_0^1 \varphi(\xi)d\xi \int_0^1 \varphi(\eta)d\eta = z_w \frac{h+H}{2} \rho_k' u_m \int_0^1 \varphi(\zeta)d\zeta \quad \text{(Eq 24)}$$

where $\varphi(\xi) = M^2/M_m^2$, $\varphi(\eta) = M^2/M_m^2$ along the axis z, $\xi = x/h$, $\eta = y/h$; $\varphi(\zeta) = M^2/M_m^2$ along the axis z, $\zeta = z / z_w$. In case of uniform distribution of gas parameters over cross-section:

$$\int_0^1 \varphi(\xi)d\xi = \int_0^1 \varphi(\eta)d\eta = \int_0^1 \varphi(\zeta)d\zeta = C = 1 \quad \text{(Eq 25)}$$

It is possible to yield:

$$z_w = \frac{h}{2}\frac{1}{1+h/H}\left(\frac{\rho_m v_m}{\rho_k'}\right) = \frac{1}{2}\frac{h}{1+h/H}\Psi \quad \text{(Eq 26)}$$

$$\Psi = \frac{(1+aM_m^2)^{0.5}\,(kM_m^2 - a)^{0.5/a}}{(cM_m)^b} \quad \text{(Eq 27)}$$

$$a = \frac{\gamma-1}{2},\ b = \frac{\gamma+1}{\gamma-1},\ c = \left(\frac{\gamma+1}{2}\right)^{0.5} \quad \text{(Eq 28)}$$

where M_m is the Mach number at the jet axis. The value Ψ at M_m = 1.8-3.1 is 0.86-0.72, i.e., approximately 0.8. The average of all data in Fig. 18 for isobaric exhaustion gives the compressed

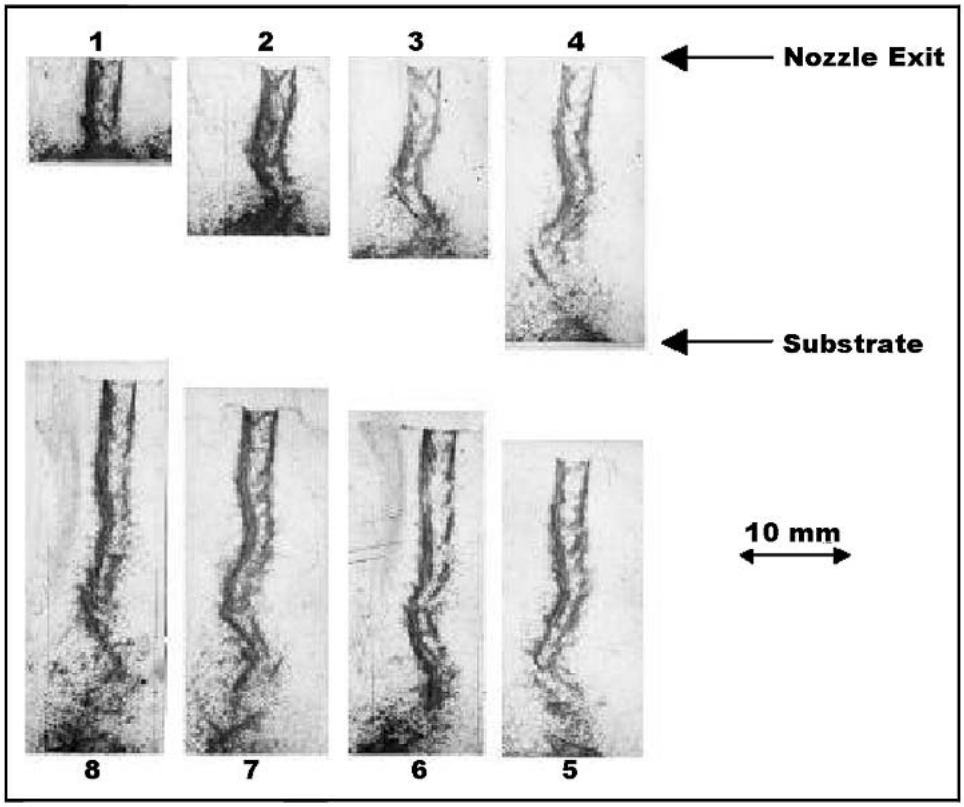

Fig. 14 Regimen of the oscillation impingement of the supersonic rectangular jet onto the obstacle mounted at 90° to jet axis; time of exposition $t = 30 \times 10^{-9}$ s, $M^* = 2.25$, $h = 3$ mm, $z_0/h = 3$ (*1*), 5 (*2*), 5,7 (*3*), 8 (*4*), 9 (*5*), 9,7 (*6*), 10,3 (*7*), 11 (*8*)

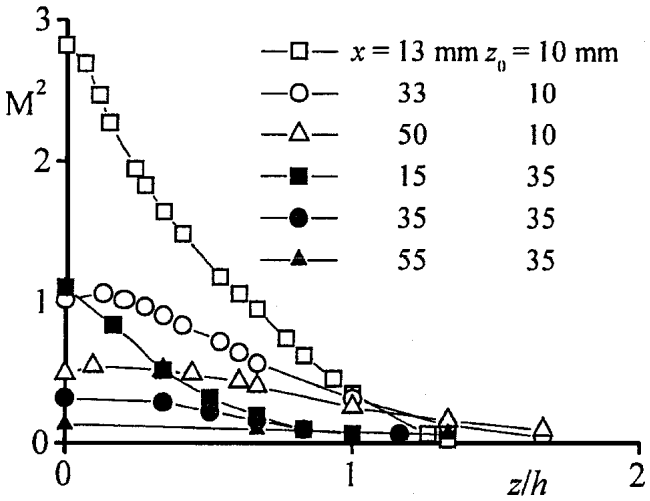

Fig. 15 Profile of the M^2 in the near-wall jet far from the critical point at the impingement onto the obstacle mounted at 90° to the jet axis

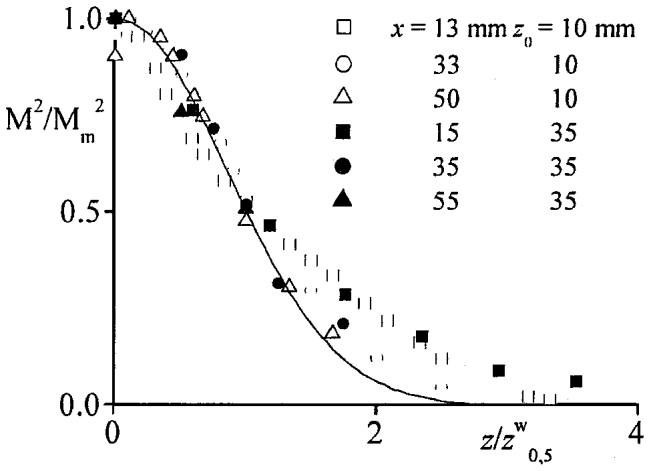

Fig. 16 Normalized profiles of the Mach numbers in the near-wall jet far from the critical point at the impingement onto the obstacle mounted at 90° to jet axis; $h = 3$ mm, $H/h = 3.3$, $M_* = 2.5$

layer thickness estimate by $0.45h$ independently on a distance in range from 0 up to $10h$.

The investigation of flow modes incipient at the interaction of the supersonic jet with a flat barrier concludes that there are four various modes: classic mode, the mode with peripheral maximum and circulate bands, the mode with oscillations of bow shock, and the mode with jet oscillations. The main parameters influencing the transition from one mode to another are jet pressure ratio, distance, and jet thickness. Classic mode occurs at near isobaric exhaustion and small distance. It allows in practice to choose the necessary parameters to avoid poorly predicted consequences of non-classic modes.

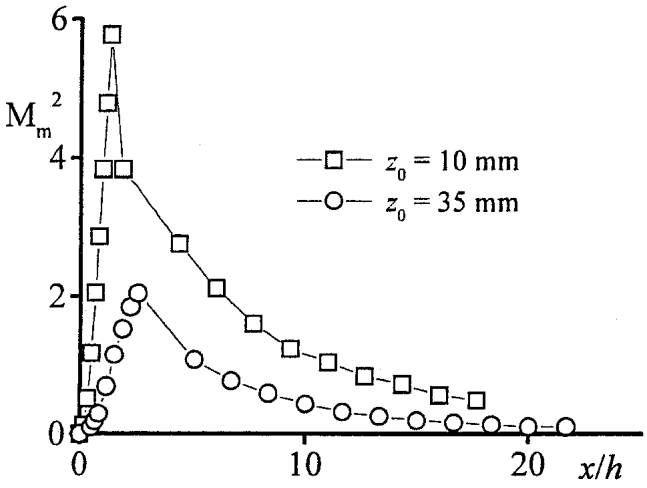

Fig. 17 Distribution of M_m^2 (x/h) along the surface of the obstacle mounted at 90° to jet axis

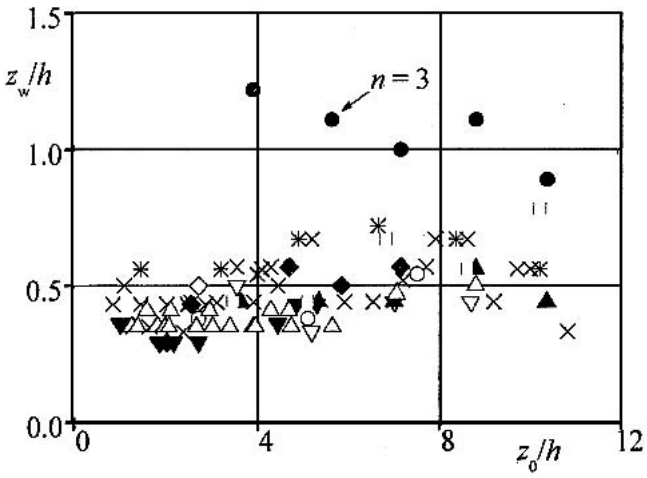

Fig. 18 Dependence of compressed layer thickness on distance; the range of varied parameters was h = 1-5 mm, H/h = 2.7-8, M = 1.8-3.1

5. Heat Transfer

For various coating processes it is important to control the temperature of the coated workpiece to ensure a required spraying mode and conditions of the workpiece surface.[51,52] For example, the use of exothermal reactions under the interaction of coating components on the spray surface in the cold spray process looks very promising for different applications. However, it is known that to initialize the synthesis reaction of the intermetallide compound it is necessary to heat the mixture of initial components up to a certain temperature.

For a rather small concentration of particles ($\varphi \leq 10^{-6}$) ordinarily used in the cold-spray process, the heat exchange between the particles and the surface is small compared with the gas-surface heat exchange. Therefore, in estimating the surface temperature, the heat exchange between the jet and the surface is considered.

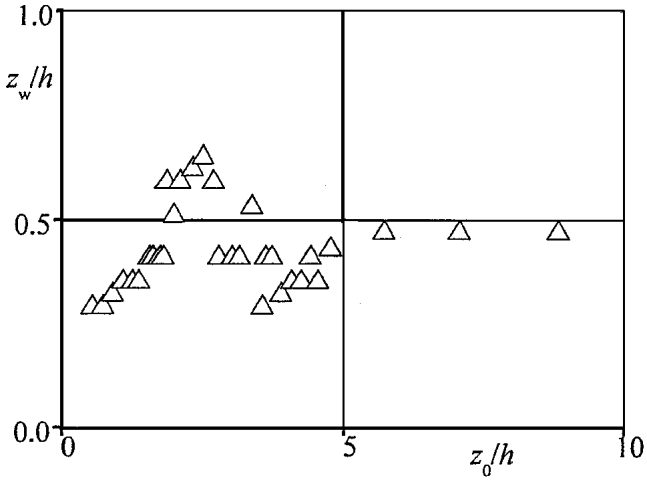

Fig. 19 Dependence of compressed layer thickness on distance at impingement of supersonic nonisobaric (n = 1.5) jet from the nozzle with parameters: h = 5, H/h = 1.68, M_* = 2.55

5.1 Method of Measurement of Heat Exchange Coefficient

For the measurement of heat exchange efficiency, a calorimetric probe inserted into a slab of thermoinsulator material flash-mounted with the surface was used. In Fig. 21, a schematic flow of a plane supersonic jet on the substrate with the indication of coordinate axes and main geometric sizes of the problem considered is shown.

Let us consider the heat exchange of the gas with the unrestricted plate of thickness δ_s. The heat exchange coefficient α and the stagnation temperature of gas T_0 are assumed to be constant in time. At the initial moment of time $t = 0$ heat exchange starts between the plate with the initial temperature T_{s_0} and gas at the boundary $z = 0$. The second boundary of the plate is considered to be thermoinsulated. Introducing non-dimensional values:

$$z = \xi\delta_s,\ t = \tau\frac{\delta_s^2}{\chi},\ T_s = T_0(1-\theta) \qquad \text{(Eq 29)}$$

non-stationary equation of heat conductivity, the initial and boundary conditions can be written as:

$$\frac{\partial\theta}{\partial\tau} = \frac{\partial^2\theta}{\partial\xi^2} \qquad \text{(Eq 30)}$$

$$\frac{\partial\theta}{\partial\xi} = \frac{\alpha\delta_s}{\lambda}\theta_w \text{ or } \xi = 0$$

$$\frac{\partial\theta}{\partial\xi} = 0 \text{ or } \xi = -1 \qquad \text{(Eq 31)}$$

$$\theta = \theta_0 = 1 - \frac{T_{s_0}}{T_0} \text{ or } \tau = 0$$

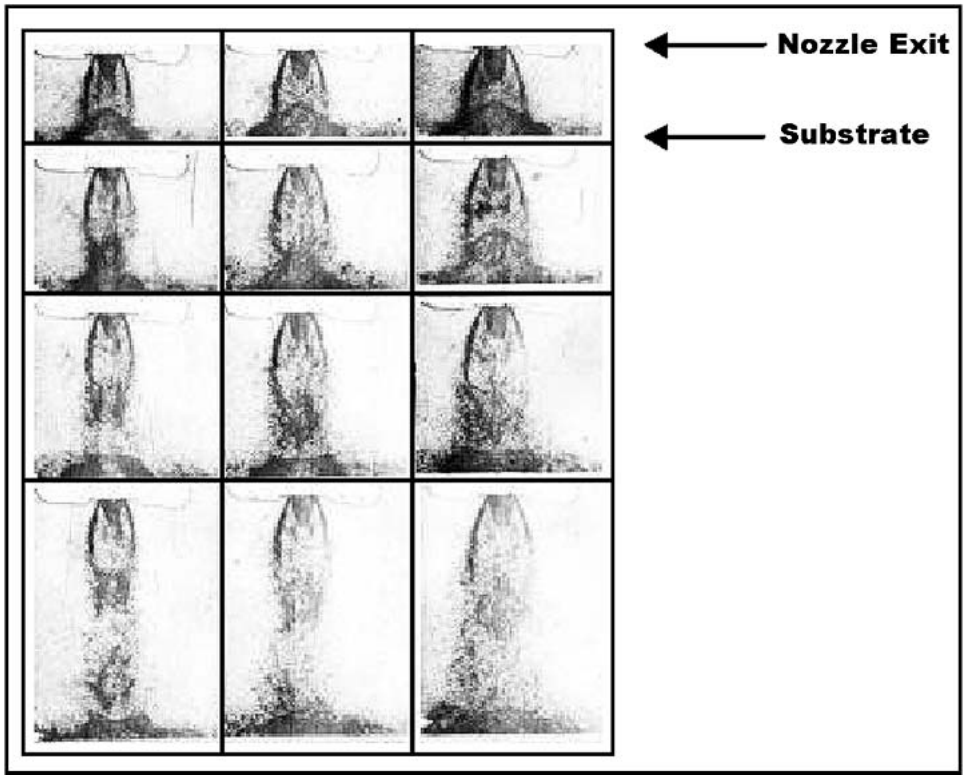

Fig. 20 Compressed layer structure (2.3×). Pressure ratio: 1st column, 2.2; 2nd, 3; 3rd, 3.5. Distance (mm): 1st row, 10; 2nd, 15; 3rd, 20; 4th, 30

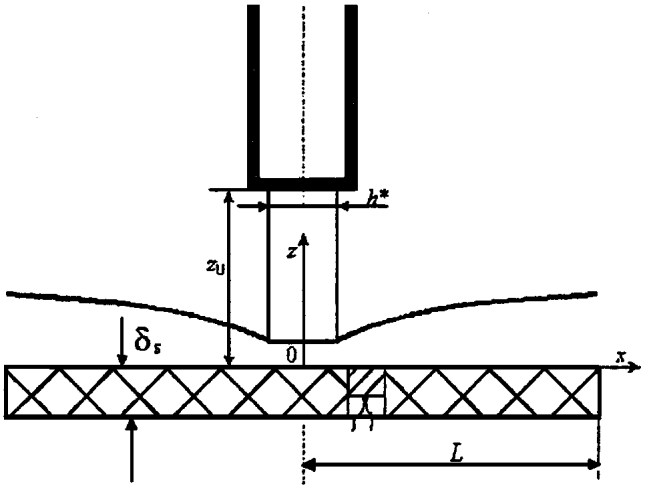

Fig. 21 Schematic flow of a plane supersonic jet on the substrate

where $\chi = \lambda/(c\rho)$ is the temperature conductivity coefficient of the plate.

The solution is presented as $\theta(\xi, \tau) = \sum_{i=1}^{\infty} f_1(\xi) \exp(-\varepsilon_i^2 \tau)$, where $f_i(\xi)$ can be presented as sum of $A \cos(\varepsilon_i \xi) + B \sin(\varepsilon_i \xi)$. Applying the boundary condition $f_i'(-1) = 0$ we find that $B = Atg(\varepsilon_i)$. From the boundary condition $f_i'(0) = -(\alpha\delta_s/\lambda) f_i(0)$, we find the condition for determining ε_i

$$\varepsilon_i tg(\varepsilon_i) = \frac{\alpha \delta_s}{\lambda} \qquad \text{(Eq 32)}$$

For $\mathrm{Fo} = (\chi\tau)/(\delta_s^2) \geq 0.3$, which corresponds to $\tau \geq [(0.3c\rho\delta_s^2)/\lambda] \approx 0.1\ c$, we can remove all terms of series except the first one, which leads to the error not more than 1%. It is obvious that in this case we can present the temperature in logarithmic form

$$\ln\left(\frac{T_0 - T_s}{T_0}\right) = a + bt \qquad \text{(Eq 33)}$$

$$b = \frac{\varepsilon_i^2 \chi}{\delta_s^2} \qquad \text{(Eq 34)}$$

For the experimental determination of α we have to solve the reverse problem. Knowing the dependence of temperature at some point of the plate on time we can represent it in coordinates

$$\ln\left(\frac{T_0 - T_s}{T_0}\right) t \qquad \text{(Eq 35)}$$

then make rms approximation of all experimental points and draw a straight line with coefficients a and b according to Eq 33. We find value ε_i by the known b from Eq 34:

$$\varepsilon_1 = \sqrt{(-b)\frac{\delta_s^2}{\chi}} \qquad \text{(Eq 36)}$$

Heat exchange coefficient is calculated from Eq 32:

$$\alpha = \frac{\lambda}{\delta_s} \varepsilon_1 tg\varepsilon_1 \qquad \text{(Eq 37)}$$

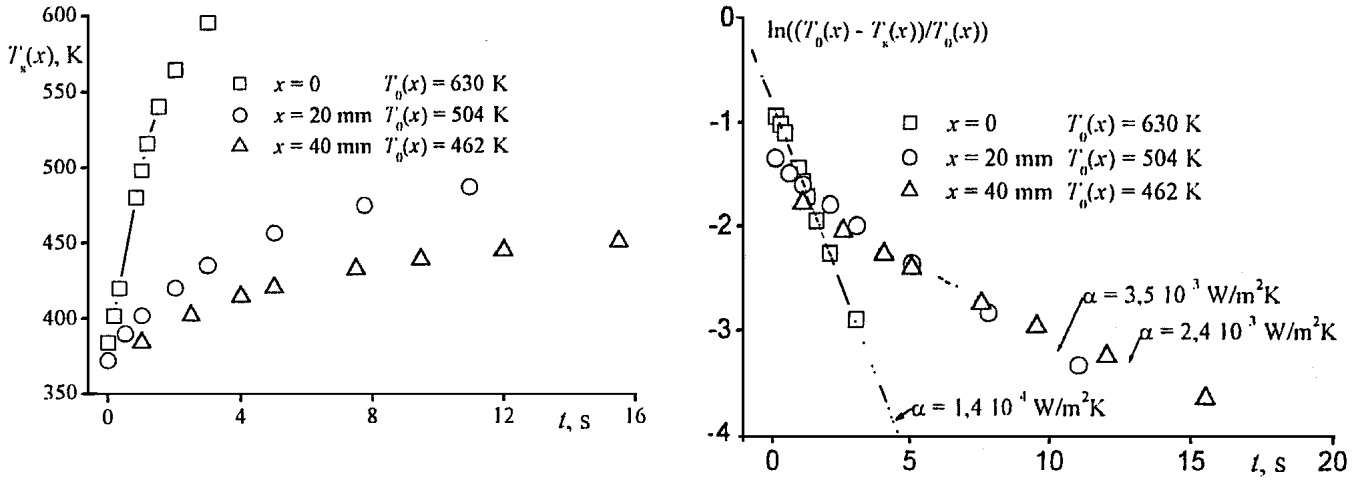

Fig. 22 Dependence of temperature on time of isobaric air jet inflow; jet thickness at the nozzle exit, $h_* = 3$ mm, $z_0 = 15$ mm

5.2 Results of the Experiments on Determining the Heat Exchange Coefficient

As an example, Fig. 22 shows the results of the experiments on determining the heat exchange coefficient of jet ($p_0 = 1.45$ MPa, $T_0^x = 630$ K stagnation temperature at the nozzle exit) with the obstacle at various distances x from the nozzle axis. Figure 22(a) shows experimental points of temperature dependence on time fixed by thermocouple on the rear side of the probe. In Fig. 22(b) the same data are presented in coordinates $\ln\{[T_0(x) - T_s(x)]/T_0(x)\}\ t$; here the approximated straight lines drawn by the experimental points are given. Besides, this figure shows heat exchange coefficients corresponding to these cases and calculated by the regression slope.

The behavior of the relative stagnation temperature in the near-wall jet is represented in Fig. 23

$$f(x/x_{0.5}) = [1 + 15(x/x_{0.5})^2]^{-0.25} \quad \text{(Eq 38)}$$

A similar distribution is preserved for a flow around a non-insulated (for example, metal) surface because the heat exchange between the air jet and the substrate surface makes a rather small part of the total transferable heat (typical values of the Stanton number are St ~ 0.01). Thus, mixing of the ambient air in the wall jet mainly determines the decreasing in the stagnation temperature along the surface.

The heat transfer coefficient at the stagnation point does not depend (in the studied range) on the jet stagnation temperature at the nozzle exit. The maximum value of the heat transfer coefficient is obtained at some distance $z_0/h^* = 5$-7, and then its decrease is observed.

The dependence of the experimentally measured (Δ) Nusselt number on the Reynolds number Re_x, calculated by the distance from the stagnation point along the coordinate x, is shown in Fig. 24(a). It is visible that the dependence of the Nusselt number proportional to the heat transfer coefficient is approximated by the formula

$$\frac{\mathrm{Nu}(x)}{\mathrm{Nu}(0)} = \left[1 + 15\left(\frac{\mathrm{Re}_x}{\mathrm{Re}_{0.5}}\right)^2\right]^{-0.25} \quad \text{(Eq 39)}$$

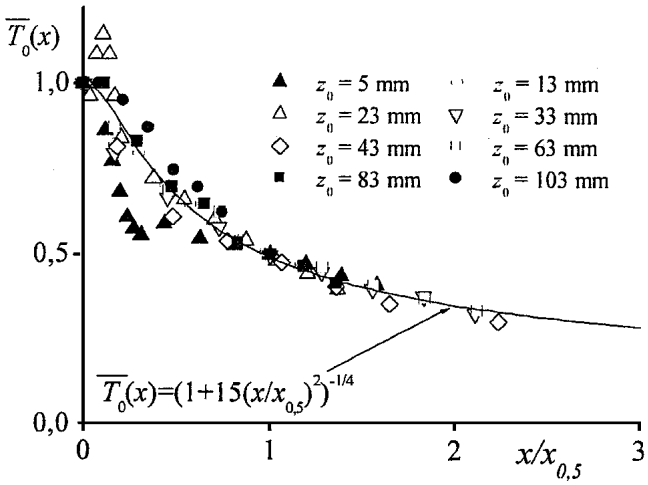

Fig. 23 Stagnation temperature in the near-wall jet, for normal flow of the air jet on the substrate, $\overline{T_0}(x) = t_0(x) - T_a/T_0^* - T_a$, $T_0^* = 550$ K, $T_a = 300$ K is the ambient temperature

which includes the entire range of x, including damping far from the stagnation point in the subsonic part of the near-wall jet, where Nu ~ $1/x^{0.5}$ according to Ref. 53.

5.3 Comparison With the Theory

For comparison, the dependence of the heat transfer coefficient on Re_x is calculated using experimental distributions of the parameters on the external boundary of the near-wall jet $M_m^2(x)$, and $T_0(x)$, by applying the formula from Ref. 56:

$$\alpha = 0.04\mathrm{Pr}^{-0.6}\,\mathrm{Re}_{xe}^{-0.2}\,\rho_e u_e c_p (T_s/T_r)^{-0.16} \quad \text{(Eq 40)}$$

where ρ_e, u_e are gas density and velocity in the near-wall jet reconstructed from $M_m^2(x)$ and $T_0(x)$ distributions. The factor $(T_s/T_r)^{-0.16}$ (T_s, T_r are substrate surface temperature and recovery temperature in the near-wall jet) makes minor influence (for conditions of our experiments, the maximum single-error cor-

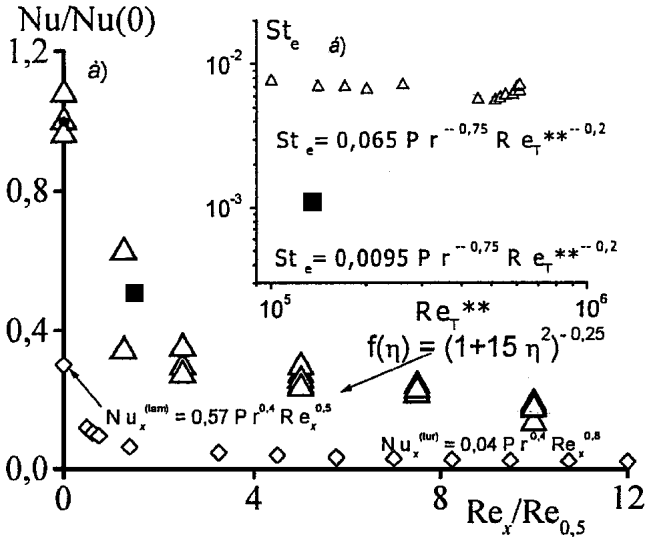

Fig. 24 Dependence of the **(a)** Nusselt and **(b)** Stanton numbers on the Reynolds number: $z_0/h^* = 5$; $Re_{0.5} = 6.8 \times 10^4$; $Nu(0) = \alpha(0)h^*/\lambda_0 = 980$; $\lambda_0 \approx 0{,}04$ W/m K; $\eta = Re_x/Re_{0.5}$

rection will make about 1.1); therefore, it was not taken into account.

In the vicinity of the stagnation point, the heat transfer coefficient was calculated using the theory of a laminar boundary layer for the flow of the jet on the substrate with allowance for velocity distributions in the vicinity of the stagnation point $u = \beta x$[53]:

$$\alpha = 0.57/\mathrm{Pr}^{0.6}\sqrt{\rho_0\beta\mu_0 c_p^2} \qquad \text{(Eq 41)}$$

A typical value for conditions of our experiment was obtained by calculation according to Eq 41, $\alpha = (3.8\text{-}4.2) \times 10^3$ W/m^{2}K at the stagnation point for $\beta = 2a_c/h_* = (2,4\text{-}3) \times 10^5$ s^{-1}.

Figure 24(a) indicates the data calculated by Eq 40 and 41 designated by rhombs. It is visible that the calculated values appear much below than the experimental results. This difference can be explained by the influence of velocity fluctuations in vicinity of the stagnation point and in the near-wall jet. For example, in Ref. 54, the influence of velocity fluctuations and other parameters is taken into account by the formula:

$$\mathrm{Nu_r}(0) = \mathrm{Nu}(0)(1 + 0.75b^{0.54}),\ b = 0.18\varepsilon v_*\sqrt{\rho_0/\beta\mu_0} \qquad \text{(Eq 42)}$$

where Nu(0) is the Nusselt number calculated disregarding turbulent oscillations, $\varepsilon = \sqrt{v^2}/v_*$ is the turbulence level, ρ_0 is the density at the stagnation point, and μ_0 is the viscosity calculated by the stagnation temperature of the flow. For the results calculated by this formula to become equal to the experimental ones, it is necessary to accept $\varepsilon = 0.25$. This value appears in the range (0.04-0.5) of ε, measured experimentally by independent methods in Ref. 54.

In Fig. 24(b), the values of the Stanton number $\mathrm{Ste} = \alpha/\rho_e u_e c_p$ are represented depending on the Reynolds number constructed by the energy loss thickness δ_T^{**}, which is calculated using to the energy equation for a turbulent boundary layer. As follows from Fig. 24(b) in this case, the experimental values appear to be greater than the calculated ones. It shows that for the flow under study it is impossible to calculate heat exchange by Eq 40 and 41 and, apparently, the model of calculation of heat exchange offered in Ref 54 is more correct and promising. However, there are difficulties in calculation and experimental measurement of velocity fluctuations, and this problem in many cases appears much more difficult than the direct measurement of the heat transfer coefficient.

5.4 Calculation of the Substrate Temperature Distribution

Experimental data allow one to determine the temperature conditions on the surface and inside the obstacle. Temperature distribution in the obstacle of length $2L$ and thickness δ_s was calculated by the joint solution of stationary equation of heat conductivity $(\partial^2 T(x, z)/\partial x^2) + (\partial^2 T(x, z)/\partial z^2) = 0$ [$T(x, z)$ is temperature in the obstacle] and the law of heat conservation in the stationary case $\int_0^L \alpha(x)[T_0(x) - T_s(x)]dx = 0$, using experimental values of stagnation temperature and heat exchange coefficient in near-wall jet. The solution was found as $T(x, z) = T_s(x) + a(x)z + b(x)z^2$, which is $\delta_s \ll L$ and low gradients of temperature in the obstacle for stationary case are justified. Boundary conditions on the surfaces $z = 0$ and $z = -\delta_s$ lead to the relation

$$\lambda\left.\frac{\partial T(x, z)}{\partial z}\right|_{z=0} = \alpha(x)[T_0(x) - T_s(x)] \rightarrow a(x) = \frac{\alpha(x)}{\lambda}[T_0(x) - T_s(x)]$$

$$\lambda\left.\frac{\partial T(x, z)}{\partial z}\right|_{z=-\delta_s} = 0 \rightarrow b(x) = \frac{a(x)}{2\delta_s} = \frac{\alpha(x)[T_0(x) - T_s(x)]}{2\delta_s\lambda}$$

As a result we have

$$T(x, z) = T_s(x) + \frac{\alpha(x)}{\lambda}[T_0(x) - T_s(x)]\left(z + \frac{z^2}{2\delta_s}\right) \qquad \text{(Eq 43)}$$

Substituting $T(x, z) = T_s(x) + a(x)z + b(x)z^2$ into the equation of heat conductivity and making necessary calculations we obtain the equation to calculate temperature of the obstacle surface:

$$\frac{\partial^2 T_s(x)}{\partial x^2} = \frac{\alpha(x)}{\delta_s}[T_0(x) - T_s(x)] \qquad \text{(Eq 44)}$$

Solving it jointly with the integral equation of heat conservation and condition of equality to zero of the first derivation from temperature at the point $x = 0$, we obtain the distribution of temperature on the obstacle surface at $0 \le x \le L$. Then by the known $T_s(x)$ we calculate the coefficients $a(x)$ and $b(x)$ and find the temperature distribution in the obstacle.

The results of calculation for $L = 100 \times 10^{-3}$ m, $T_0^* = 1200$ K, $\delta_s = 3$ mm are given in Fig. 25. Figure 25(a) presents data on the temperature of obstacle surfaces made of different materials.

The conducted calculations show that a considerable decrease in surface temperature [for the materials with $\lambda \ge 40$ W/(m · K.)] in comparison with the stagnation temperature of the inflow jet takes place due to redistribution of heat inside the obstacle. As it is seen from Fig. 25(b), at the initial region ($0 \le$

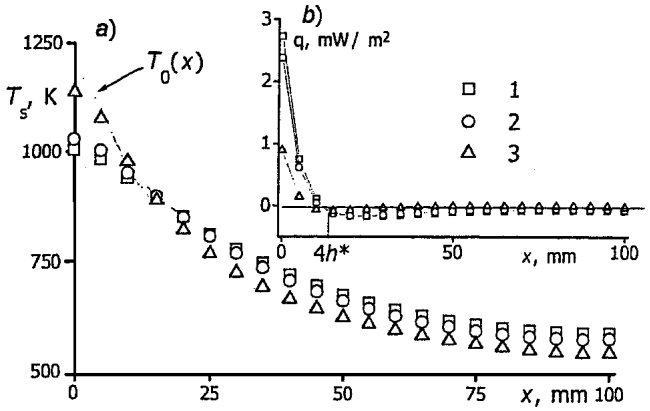

Fig. 25 Distribution of the **(a)** surface temperature and **(b)** heat flux on various substrates: 1, Cu (λ = 350 W/m K); 2, Al (λ = 250 W/m K); 3, steel (λ = 40 W/m K)

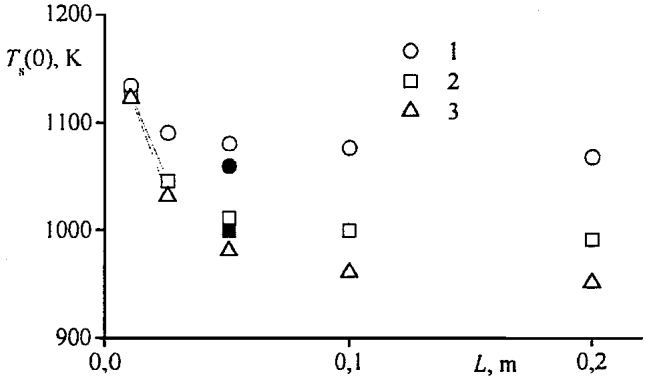

Fig. 26 Dependence of copper substrate surface temperature in the spray spot ($x = 0$) on its length: 1, $\delta_s = 1$ mm; 2, $\delta_s = 3$ mm; 3, $\delta_s = 5$ mm

$x \leq 4h^*$) heat comes into the obstacle, at large distances the process is reversed; heat comes from the obstacle into the near-wall jet.

The dependence of surface temperature in the sprayed spot ($x = 0$) on the size of the obstacle at its various thickness δ_s (Fig. 26) is constructed by the results of calculations. It is seen that when the obstacle length grows up to (15-20)h_* the temperature of the surface in its center falls considerably; the greater it is, the more it falls. Further growth of the obstacle length does not affect the surface temperature in its center. Tests (signs ●,■) shows good agreement of the measured values of the surface temperature near the critical point with the calculated ones, which confirms the correctness of the assumptions and allows one to apply the presented model of heat exchange in practical evaluations.

From Eq 43 ΔT_{max}, i.e., maximum difference of surface temperatures at $z = 0$ and $z = -\delta_s$, can be evaluated. We obtain

$$\Delta T_{max} = \frac{\alpha(0)\delta_s}{2\lambda}[T_0(0) - T_s(0)], \qquad \text{(Eq 45)}$$

where at $\Delta T_{max} \approx 20$ K for calculation presented in Fig. 25(a). In other words temperatures of surfaces $z = 0$ and $z = -\delta_s$ do not differ.

Thus, the distributions of stagnation temperature and heat exchange coefficient in near-wall jet at different distances from the supersonic nozzle exit of rectangular section to the obstacle are obtained experimentally. It is shown that experimental values of the heat exchange coefficient are considerably higher than the calculated ones. This difference can be explained by the velocity fluctuations near the critical point in the near-wall jet.

Applying the experimental data on stagnation temperature and heat exchange coefficient the temperature of the obstacle in the stationary case is calculated and it is shown that due to heat redistribution inside the obstacle, for heat-conducting materials [$\lambda \geq 40$ W/(m K)] the surface temperature in the sprayed spot considerably decreases in comparison with the stagnation temperature. In particular, this effect should be taken into account to improve the regimes of spraying with excitation of reactions of synthesis on the surface, as in this case temperature is the most important parameter influencing initiation of reactions.

6. Conclusion

Some aspects of gas dynamics of the cold spray process were studied including the flow inside the nozzle and outflow of the jet, as well as the effects of the interaction of the supersonic jet with the obstacle. These studies were conducted with the supersonic nozzles with a rectangular section and a Mach number at the nozzle exit ranging between 2 and 3.5.

It is experimentally shown that the boundary layer on the walls of the rectangular supersonic nozzles of large length to width ratio exerts a significant effect on the flow parameters. In particular, the Mach number at the nozzle exit is reduced by 10-20% from the one calculated for an isentropic flow. The displacement thickness and the boundary layer thickness are estimated. Methods of calculation of the parameters in the flow core are suggested and it is shown that the Mach number ratio depends mainly on the ratio of the nozzle thickness h to its length L. For $h/L \leq 0.025$, the effect of overlap of boundary layers from the opposite walls takes place.

The self-similarity of M^2, ΔT_0, and v profiles of the jet is verified. The region of self-similarity begins at a certain distance from the nozzle exit and extends downstream without any limitations. The transition through the sonic lines does not have any effect on the profiles of parameters. It is found that the initial nonuniformity of gas parameters at the nozzle exit leads to a more smooth transition from initial to basic region of the jet in the longitudinal distribution of M^2.

The conducted studies have shown that various modes of the interaction of the supersonic gas jet of rectangular section with the flat substrate under the conditions of the cold spray process can take place: classic mode and the mode with jet oscillations. The main parameters influencing the transition from one mode to another are jet pressure ratio, distance, and jet thickness. Classic mode occurs at near isobaric exhaustion and small distance.

It is shown that the distribution of pressure on the surface of the obstacle along the smaller size of nozzle is self-similar in the classic regimen of the impingement and does not depend on the

angle of impacting at $\varphi = 50\text{-}90°$. The critical parameters of the gas, when it accelerates along the surface, are reached near the boundary of the falling jet. Within a small distance of the obstacle from the nozzle exit ($z_0/h \leq 5$) the gas parameters can be considered constant and equal to the parameters at the exit. According to the experimental data compressed layer thickness is around $0.45h$ in range of the distance $0\text{-}10h$. The study of the near-wall jet has shown that the profiles of velocity and the Mach number are self-similar, and maximum gas velocity achieves at $(2\text{-}3)h$.

The distributions of stagnation temperature and heat exchange coefficient in near-wall jet at different distances of the nozzle exit are measured. It is shown that experimental values of the heat exchange coefficient are considerably higher than the calculated ones. This difference can be explained by the velocity fluctuations near the critical point and in the near-wall jet. The temperature of the obstacle in the stationary case is calculated, and it is shown that due to heat redistribution inside the obstacle for heat-conducting materials [$\lambda \geq 40$ W/(m K)], the surface temperature in the sprayed spot considerably decreases in comparison with the stagnation temperature.

Thus, obtained results are important for understanding gas-dynamic and thermal effects taking place under the Cold Spray process and can be used for the optimization of the process and development of various technologies.

References

1. A.P. Alkimov, V.F.Kosarev, N.I. Nesterovich, and A.N. Papyrin: "Method of Applying Coatings," Russian Patent No. 1618778, Sept 8, 1990 (Priority of the Invention: Jun 6, 1986).
2. A.P. Alkhimov, V.F. Kosarev, N.I. Nesterovich, A.N. Papyrin, and M.M. Shushpanov: "Device for Applying Coatings," Russian Patent No. 1618777, Sept 8, 1990 (Priority of the Invention: Jun 18, 1986).
3. A.P. Alkhimov, V.F. Kosarev, N.I. Nesterovich, and A.N. Papyrin: "Method of Applying of Metal Powder Coatings," Russian Patent No. 1773072, Jul 1, 1992 (Priority of the Invention: Oct 5, 1987).
4. A.P. Alkhimov, V.F. Kosarev, and A.N. Papyrin: "A Method of Cold Gas-Dynamic Deposition," *Sov. Phys. Dokl.,* 1990, *35*(12), pp. 1047-49 (Transl: American Inst. of Phys., 1991).
5. A.N. Papyrin, A.P. Alkhimov, and V.F. Kosarev: "Cold Gas-Dynamic Spray Method" in *New Materials and Technologies: Theory and Practice of Hardening Materials in Extreme Processes,* Nauka, Novosibirsk, Russia, 1992, pp. 146-68.
6. A.P. Alkimov, A.N. Papyrin, V.F. Kosarev, N.I. Nesterovich, and M.M. Shushpanov: "Gas Dynamic Spraying Method for Applying a Coating," U.S. Patent No. 5,302,414, Apr 12, 1994, Re-examination Certificate, Feb 25, 1997.
7. A.P. Alkimov, A.N. Papyrin, V.F. Kosarev, N.I. Nesterovich, and M.M. Shushpanov: "Method and Device for Coating," European Patent No. 0484533, Jan 25, 1995.
8. R.C. McCune, A.N. Papyrin, J.N. Hall, W.L. Riggs, and P.H. Zajchowski: "An Exploration of the Cold Gas-Dynamic Spray Method for Several Materials Systems" in *Advances in Thermal Spray Science and Technology,* C.C. Berndt and S. Sampath, ed., ASM International, Materials Park, OH, 1995, pp. 1-5.
9. R.C. McCune, W.T. Donoon, E.L. Cartwright, A.N. Papyrin, E.F. Rybicki, and J.R. Shadley: "Characterization of Copper and Steel Coatings Made by the Cold Gas-Dynamic Spray Method" in *Thermal Spray: Practical Solutions for Engineering Problems,* C.C. Berndt, ed., ASM International, Materials Park, OH, pp. 397-403, 1996.
10. A.P. Alkhimov, S.V. Klinkov, V.F. Kosarev, and A.N. Papyrin: "Gas-Dynamic Spraying: Study of Plane Supersonic Two-Phase Jet," *J. Appl. Mech. Tech. Physics,* 1997, *38*(2), pp. 176-83.
11. A.P. Alkhimov, V.F. Kosarev, and A.N. Papyrin: "Gas-Dynamic Spraying. Experimental Study of Spraying Process," *J. Appl. Mech. Tech. Physics,* 1998, *39*(2), pp. 183-88.
12. A.P. Alkhimov, V.F. Kosarev, and A.N. Papyrin: "Spraying Current Conducting Coatings on Electro-Technical Units by CGS Method" *Proceedings of United Thermal Spray Conference,* Dusseldorf, Germany, E. Lugscheider and P.A. Kammer, ed., ASM International, Materials Park, OH, 1999, pp. 288-90.
13. A.P. Alkimov, A.I. Gulidov, V.F. Kosarev, and N.I. Nesterovich: "Specific Features of Microparticle Deformation Upon Impact on a Rigid Barrier," *J. Appl. Mech. Tech. Physics,* 2000, *41*(1), pp. 204-09.
14. A.P. Alkhimov, S.V. Klinkov, and V.F. Kosarev: "Impingement of a Supersonic Jet of a Rectangular Section on Flat Barrier," *Thermophysics and Aeromechanics,* 2000, *7*(2), pp. 221-28.
15. A.P. Alkhimov, S.V. Klinkov, and V.F. Kosarev: "Study of Heat Exchange of Supersonic Plane Jet With Obstacle at Gas-Dynamic Spraying," *Thermophysics and Aeromechanics,* 2000, *7*(3), pp. 375-82.
16. A.N. Papyrin, A.P. Alkhimov, V.F. Kosarev, and S.V. Klinkov: "On the Interaction of a Supersonic Gas Jet With a Substrate Under the Cold Spray Process" in *Proceedings of International Thermal Spray Conference,* Singapore, May 28-30, C. Berndt, K. Knor, and E. Lugscheider, ed., ASM International, Materials Park, OH, 2001, pp. 423-31.
17. A.N. Papyrin: "Cold Gas Dynamic Spraying: What Is It?," *ASM International Materials Solutions Conference,* Rosemont, Illinois, Oct 12-15, ASM International, Materials Park, OH, 1998.
18. A.N. Papyrin, A.P. Alkhimov, V.F. Kosarev, and S.V. Klinkov: "On Some Aspects of Gas-Dynamics of the Cold Spray Process," *International Thermal Spray Conference,* Montreal, Canada, May 8-11, ASM International, Materials Park, OH, 2000.
19. R.C. Dykhuizen and M.F. Smith: "Gas Dynamic Principles of Cold Spray," *J. Thermal Spray Technol. 7*(2), 1998, pp. 205-12.
20. D.L. Gilmore, R.C. Dykhuizen, R.A. Neiser, T.J. Roemer, and M.F. Smith: "Particle Velocity and Deposition Efficiency in the Cold Spray Process," *J. Therm. Spray Technol.,* 1998, *8*(4), pp. 559-64.
21. R.C. Dykhuizen, M.F. Smith, R.A. Neiser, D.L. Gilmore, X. Jiang, and S. Sampath: "Impact of High Velocity of Cold Spray Particles," *J. Therm. Spray Technol.,* 1998, *8*(4), pp. 559-64.
22. M.F. Smith, J.E. Brockmann, R.C. Dykhuizen, D.L. Gilmore, R.A. Neiser, and T.J. Roemer: "Cold Spray Direct Fabrication-High Rate, Solid State Material Consolidation" in *MRS Symposium Proceedings 542,* Materials Research Society, Pittsburgh, PA, 1999, pp. 65-67.
23. J.E. Brockmann, R.C. Dykhuizen, R. Cote, and T. Roemer: "Aerodynamic Focusing of Large Particles," *J. Aerosol. Sci.,* 1998, *29* Suppl. 1, pp. S1067-S1068.
24. D.L. Gilmore, R.C. Dykhuizen, R.A. Neiser, and M.F. Smith: "Analysis of the Critical Velocity for Deposition in the Cold Spray Process," *ASM International Material Solutions Conference,* Cincinnati, OH, Nov 2-4, ASM International, Materials Park, OH, 1999.
25. D.L. Gilmore and R.A. Neiser: "Effect of Particle Velocity on Coating Properties in the Cold Spray Process," *ASM International Materials Solutions Conference,* St. Louis, MO, Oct 9-12, ASM International, Materials Park, OH, 2000.
26. R.B. Bhagat, M.F. Amateau, A.N. Papyrin, J.C. Conway, Jr., B. Stutzman, and B. Jones: "Deposition of Nickel-Aluminum Bronze Powder by Cold Gas- Dynamic Spray Method on 2618 Al for Developing Wear Resistant Coatings" in *Proceedings of 10th National Thermal Spray Conference,* C.C. Berndt, ed., ASM International, Materials Park, OH, 1997, pp. 361-67.
27. A.E. Segall, A.N. Papyrin, J.C. Conway, Jr., and D. Shapiro: "A Cold-Gas Spray Coating Process for Enhancing Titanium," *JOM,* 1998, *50*(9), pp 52-54.
28. D.H. Stiver, A.N. Papyrin, M.F. Amateau, and R.B. Bhagat: "Aluminum Based Wear Resistant Coatings by Cold Spray," *ASM International Materials Solutions Conference,* Cincinnati, OH, Nov 2-4, ASM International, Materials Park, OH, 1999.
29. A.N. Papyrin, D.H. Stiver, R.B. Bhagat, and M.F. Amateau: "Wear Resistant Coatings by Cold Gas Dynamic Spray," *International Thermal Spray Conference,* Montreal, Canada, May 8-11, ASM International, Materials Park, OH, 2000.
30. J. Karthikeyan, A. Kay, J. Lindeman, R.S. Lima, and C.C. Berndt: "Cold Spray Processing of Titanium Powder" in *Thermal Spray: Surface Engineering via Applied Research,* C.C. Berndt, ed., ASM International, Materials Park, OH, 2000, pp. 255-62.
31. J. Karthikeyan, A. Kay, and J. Lindeman: "Cold-Spray Processing of Stainless Steel Powder," *ASM International Materials Solutions Con-*

ference, St. Louis, MO, Oct 9-12, ASM International, Materials Park, OH, 2000.
32. R.C. McCune, R.P. Cooper, and O.O. Popoola: "Post-Processing of Cold-Spray Deposits of Copper and Iron," *International Thermal Spray Conference,* Montreal, Canada, May 8-11, C. Berndt, ed., ASM International, Materials Park, OH, 2000.
33. H. Richter and G. May: " Fluid Mechanic and Thermal Aspects of High Velocity Spraying," *Proceedings of the 5th Colloquium on HVOF Spraying,* Erding, Germany, C. Penszior and P. Heinrich, ed., Gemeinschaft Thermisches Spritzen e.V., 2000, pp. 19-28.
34. V. Shukla and G. Elliott: "The Fluid Dynamics of Cold Gas Dynamic Spray," *ASM International Materials Solutions Conference,* St. Louis, MO, Oct 9-12, ASM International, Materials Park, OH, 2000.
35. H. Kreye and T. Stoltenhoff: "Cold Spray–Study of Process and Coatings Characteristics" in *Thermal Spray: Surface Engineering via Applied Research,* C.C.Berndt, ed., ASM International, Materials Park, OH, 2000, pp. 419-22.
36. T. Stoltenhoff and H. Kreye: "Cold Spraying—From Thermal Spraying to High Kinetic Energy Spraying," *Proceedings of the 5th Colloquium on HVOF Spraying,* Erding, Germany, C. Penszior and P. Heinrich, ed., Gemeinschaft Thermisches Spritzen e.V., 2000, pp. 29-38.
37. T. Stoltenhoff and H. Richter: "Application of Computational Fluid Dynamics for the Evaluation of the Cold Spray Process Parameters," *International Thermal Spray Conference,* Montreal, Canada, May 8-11, C. Berndt, ed., ASM International, Materials Park, OH, 2000.
38. J. Vlcek, H. Huber, H. Voggenreiter, A. Fischer, E. Lugscheider, H. Hallen, and G. Pache: "Kinetic Powder Compaction Applying the Cold Spray Process. A Study on Parameters," in *Proceedings of the International Thermal Spray Conference,* Singapore, May 28-30, C. Berndt, K. Knor, and E. Lugscheider, ed., ASM International, Materials Park, OH, 2001.
39. K. Sakaki: "Numerical Simulation of Thermodynamical Behavior of Gas and Spray Particles in the Cold Spray," *ASM International Material Solutions Conference,* St. Louis, MO, Oct 9-12, C. Penszior and P. Heinrich, ed., Gemeinschaft Thermisches Spritzen e.V., 2000.
40. A.O. Tokarev: "Structure of Aluminum Powder Coatings Prepared by Cold Gas-Dynamic Spraying," *Met. Sci. Heat Treat,* 1996, *38*(3-4), pp. 136-39.
41. T. Shmyreva, E. Popov, A. Papyrin, and E. Smith: "Nanostructured Hydroxapatite Powders and Coatings," *Proceedings of United Thermal Spray Conference,* Dusseldorf, Germany, E. Lugscheider and P.A. Kammer, ed., ASM International, Materials Park, OH, 1999, pp. 736-39.
42. D.R. Bartz: "An Approximate Solution of Compressible Turbulent Boundary-Layer Development and Convective Heat Transfer in Convergent-Divergent Nozzles," *Trans. ASME,* 1978, *77*(8), pp. 1235-45.
43. H. Schlichting: *Boundary Layer Theory,* McGraw Hill, New York, 1968.
44. A.P. Alkhimov, S.V. Klinkov, and V.F. Kosarev: "The Features of Cold Spray Nozzle Design," *J. Thermal Spray Technol.,* 2001, *10*(2), p. 375-81.
45. M.E. Deich and A.E. Zaryankin: *Gas Dynamics of Diffusers and Output Tubes of Turbomachines,* Energiya, Moscow, 1970.
46. G.I. Abramovich: *Applied Gas Dynamics,* Nauka, Moscow, 1969.
47. A.S. Ginevsky: *Turbulent Jet and Wake Theory. Integral Methods of Calculation,* Mashinostroenie, Moscow, 1969.
48. G.N. Abramovich: *Turbulent Jet Theory,* Nauka, Moscow, 1984.
49. L.A. Vulis and V.P. Kashkarov: *Viscous Jet Theory,* Nauka, Moscow, 1965.
50. I.A. Belov: *Interaction of the Non-Uniform Flows With the Obstacles,* Mashinostroenie, Leningrad, 1983.
51. V.V. Kudinov, P.Y. Pekshev, and V.E. Belashenko: *Plasma Spraying,* Nauka, Moscow, 1990, p. 407.
52. H.M. Shorshorov and Y.A. Harlamov: *Physico-Chemical Fundamentals of Detonation Spraying,* Nauka, Moscow, 1978.
53. B.N. Yudaev, M.S. Michailov, and V.K. Savin: *Heat Exchange at Jet–Obstacle Interaction,* Mashinostroenie, Moscow, 1977.
54. I.A. Belov: *Interaction of Irregular Flows With Obstacles,* Mashinostroenie, Leningrad, 1983.
55. E.P. Volchkov and S.V. Semenov: *Fundamentals of Boundary Layer Theory,* Institute of Thermophysics, SB RAS, Novosibirsk, 1994.
56. Yu. V. Lapin: *Turbulent Boundary Layer in Supersonic Gas Flows,* Nauka, Moscow, 1970.